ADIR: Angular Differential Imaging applied to Rhapsodie(Reconstruction of High-contrAst Polarized SOurces and Deconvolution for cIrcumstellar Environments)

Vincent Tardieux
(supervisor: Laurence Denneulin)

Technical Report n^o202407-techrep-tardieux, July 2024
revision 2278677

Observing circumstellar environments offers insights into the process of planet formation. Such environments refers to the regions surrounding young stars where various physical processes occur, such as the evolution of dust and gas circumstellar disk and the planets fomation.

Leveraging the capabilities of the ESO-VLT SPHERE IRDIS instrument, we employ polarimetric imaging to disentangle faint, polarized signals from the overwhelming glare of the host star, which is unpolarized.

Here, we aim to enhance RHAPSODIE (Reconstruction of High-contrAst Polarized SOurces and Deconvolution for cIrcumstellar Environments), an "inverse problem" approach for reconstructing images of linearly polarized light and corresponding polarization angle maps.

Our objective is to enhance RHAPSODIE to enable the reconstruction of images from the non-polarized scattered light of the sources utilizing data obtained with pupil tracking mode.

This paper presents ADIR, a method for Angular Differential Imaging applied to RHAPSODIE, which aims to reconstruct high-contrast polarized sources and deconvolute circumstellar environments. The primary objective is to disentangle a disk's light from its starlight.

Observer les environnements circumstellaires offre des perspectives précieuses sur le processus de formation des planètes. Ces environnements font référence aux régions entourant les jeunes étoiles où divers processus physiques se produisent, tels que l'évolution de la poussière et du gaz dans le disque circumstellaire ainsi que la formation des planètes.

En tirant parti des capacités de l'instrument IRDIS du VLT de l'ESO, nous utilisons l'imagerie polarimétrique pour démêler les signaux polarisés faibles de l'éclat écrasant de l'étoile hôte, qui est non polarisée.

Nous visons ici à améliorer RHAPSODIE (Reconstruction of High-contrAst Polarized SOurces and Deconvolution for cIrcumstellar Environments), une approche de "problème inverse" pour reconstruire des images de lumière polarisée linéairement et des cartes correspondantes des angles de polarisation.

Notre objectif est d'améliorer RHAPSODIE afin de permettre la reconstruction d'images à partir de la lumière diffusée non polarisée des sources en utilisant les données obtenues en mode suivi de pupille.

Cet article présente ADIR, une méthode d'imagerie différentielle angulaire appliquée à RHAPSODIE, qui vise à reconstruire des sources polarisées à fort contraste et à déconvoluer les environnements circumstellaires. L'objectif principal est de démêler la lumière d'un disque de celle de son étoile.

Keywords

Circumstellar environment, Proto-planetary disk, Planet formation, Angular Differential Imaging, Astrophysics

Laboratoire de Recherche de l'EPITA
14-16, rue Voltaire – FR-94276 Le Kremlin-Bicêtre CEDEX – France
Tél. +33 1 53 14 59 22 – Fax. +33 1 53 14 59 13
vincent.tardieux@epita.fr – http://www.lre.epita.fr/

1 State-of-the-art

Observing circumstellar environments requires advanced methods and instruments to disentangle the light from stars and their surrounding disks. Two primary methods used in this field are Angular Differential Imaging (ADI) and Differential Polarization Imaging (DPI).

1.1 Methods to Disentangle Light

Angular Differential Imaging (ADI)

Angular Differential Imaging (ADI) is a technique that takes advantage of the field rotation to separate the light from the star and its surrounding disk. By capturing multiple images over time as the field of view rotates, ADI can enhance the visibility of faint structures around bright stars Marois (2006).

Differential Polarization Imaging (DPI)

Differential Polarization Imaging (DPI) utilizes the polarization properties of light to distinguish between the unpolarized light of a star and the polarized light scattered by the surrounding disk. This method is crucial for studying the composition and structure of circumstellar environments de Boer et al. (2020).

1.2 State-of-the-Art Instrument

One of the leading instruments for observing circumstellar environments in dual-beam polarimetric imaging mode is the ESO/VLT SPHERE IRDIS. This instrument is specifically designed to achieve high-contrast imaging, enabling detailed observations of faint circumstellar disks and exoplanets around bright stars de Boer and Langlois (2020).

1.3 State-of-the-Art Method to Extract Polarized Light

The Double Difference method is currently the state-of-the-art technique for extracting polarized light. This method involves taking multiple polarized images at different orientations and subtracting them to isolate the polarized component of the light Tinbergen (2005).

1.4 RHAPSODIE: Challenging the State-of-the-Art

Inverse Problem Approach

RHAPSODIE is an approach that challenges the existing state-of-the-art by using an inverse problem framework. This method aims to improve the extraction of polarized light by accounting for the statistical properties of the data Denneulin (2021).

Direct Model of the Data

RHAPSODIE incorporates a direct model of the data, which includes factors such as blur, polarization variations, translations, and rotations. This comprehensive modeling helps in accurately separating the light from the disk and the star Denneulin (2021).

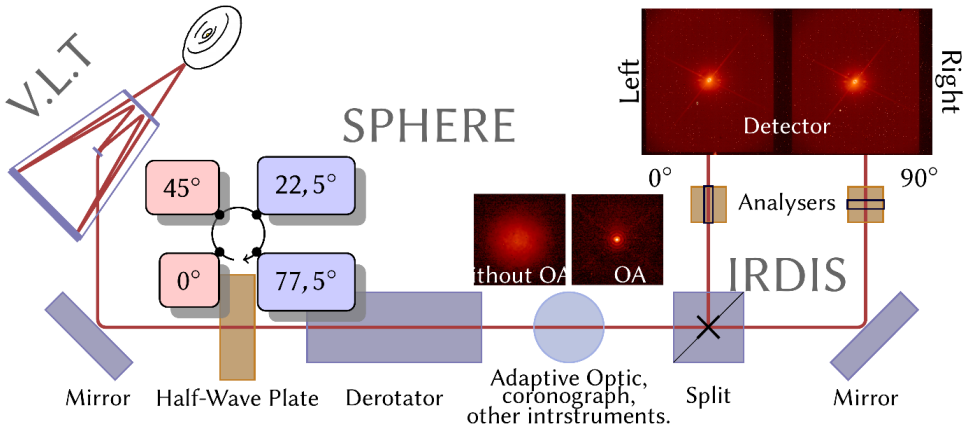

Figure 1: Scheme of the ESO/VLT SPHERE IRDIS Instrument

1.5 Current Limitations

Despite advancements, a significant limitation in current methods is that they only provide the polarized light of the disk. This limitation hampers the comprehensive study of the circumstellar environment.

1.6 My Contribution

To address the limitations, my contribution involves combining Angular Differential Imaging (ADI) with Differential Polarization Imaging (DPI). This combined approach aims to improve the separation of the star's light and the disk's light, providing a more detailed understanding of circumstellar environments.

2 ESO/VLT SPHERE IRDIS

The ESO/VLT SPHERE IRDIS instrument (figure 1) is designed for high-contrast imaging and spectroscopy, particularly for studying circumstellar environments around young stars. This section breaks down the components and explains how the instrument works part by part.

- **VLT (Very Large Telescope):** The light from the star system is collected by the VLT, which is equipped with a large mirror to gather and focus light.
- **Half-Wave Plate:** This component is used to rotate the polarization plane of the incoming light. It has multiple positions (0°, 22.5°, 45°, 77.5°) to achieve different polarization states.
- **Derotator:** The derotator compensates for the field rotation that occurs as the telescope tracks objects across the sky. However, for Angular Differential Imaging (ADI), the derotator is turned off to allow the field of view to rotate naturally, which is essential for distinguishing the star's light from the disk's light by taking advantage of the sky rotation.
- **Adaptive Optics (AO), Coronagraph, and Other Instruments:** The AO system corrects for distortions caused by Earth's atmosphere in real-time, improving image quality. The

coronagraph blocks the star's light to enhance the visibility of the surrounding disk and planets.

- **Split:** The light path is split into two beams: one for the left detector and one for the right detector.
- **Analysers:** The analysers, placed in each beam path (left and right), are used to separate the light into its different polarization components (0° and 90°).
- **IRDIS (Infra-Red Dual-beam Imager and Spectrograph):** This is the main imaging component that captures the dual-beam images. It includes two detectors (left and right) to simultaneously record two orthogonal polarization states of the light.

Since we are using ADI, the derotator is turned off. This allows the field of view to rotate over time as the telescope tracks the object. By capturing a series of images over time, we can later combine these images in a way that the star's position remains fixed while the surrounding environment rotates. This helps in differentiating the light from the disk (which rotates) and the star (which remains stationary).

The half-wave plate and analysers work together to analyze the polarization state of the incoming light. By rotating the half-wave plate to different angles and using the analysers, the instrument can measure the Stokes parameters (I, Q, U) that describe the polarization state. This information is crucial for understanding the scattering properties of the circumstellar disk.

This detailed setup allows astronomers to achieve high-contrast imaging, necessary for studying faint structures like circumstellar disks and exoplanets around bright stars.

3 Symbol table

Table 1: Symbols

Symbol	Description
$d_{j,k,m}$	Measured data
$I^{det}_{j,k,m}$	Model of the data
$H_{j,k,m,n}$	Instrumental PSF
A_k	Instrumental blur
$T_{j,k}$	Geometrical modifications
$\sum_{j,k,m}$	Variance of data
$v_{j,k,l}$	Polarization effects
I^u	Unpolarized intensity
I^u_{disk}	Disk's unpolarized intensity
I^u_{star}	Star's unpolarized intensity
I^p	Polarized intensity
I^p_{disk}	Disk's Polarized intensity
θ	Polarization angle
$S = (I^u_{star}, I^u_{disk}, I^p_{disk}, \theta)$	Stokes parameters
X	Parameters of interest
$\hat{X}$	Estimated parameters
f_{data}	Data fidelity term
$W_{j,k,m}$	Weights
$J_{O->B}$	Jacobian of $I^{det}_{j,k}$
λf_{prior}	Regularization term
Indices	
$j \in \{1, 2\}$	Polarizer of the analyser set
$k \in [\![1, K]\!]$	Data frame in the sequence
$l \in [\![1, L]\!]$	Component of the parameter of interest
$m \in [\![1, M]\!]$	Pixel in data sub-image
$n, n' \in [\![1, N]\!]$	Pixel in restored model maps
ρ	Param. to regularize $(I^u_{star}, I^u_{disk}, I^p_{disk}, \theta)$

4 Differential Polarization Imaging in the context of ADIR

Differential Polarization Imaging (DPI) is a technique used to observe and analyze polarized light from astronomical sources. The Stokes parameters (**S** = (I, Q, U)) are utilized, where $I = I^u + I^p$. The components I^u and I^p are given by $I^u = I^u_{star} + I^p_{disk}$ and $I^p = \sqrt{Q^2 + U^2}$, with $Q = I^p \cos(2\theta)$ and $U = I^p \sin(2\theta)$.

5 Method

5.1 Direct Model

We define the direct model according to equation (9) of the paper RHAPSODIE:

$$I^{det}_{j,k,m} = \sum_{l=1}^{4} \sum_{n=1}^{N} v_{j,k,l}\ H_{j,k,m,n}\ S_{l,n} \tag{1}$$

We can now define $I^u = I^u_{disk} + I^u_{star}$ et $I^p = I^p_{disk} + I^p_{star}$

Furthermore we assume that star's light is entirely non polarised thus $I^p_{star} = 0$ thus $I^p = I^p_{disk}$.

By explicitly stating the Stokes parameters in a basis we will call S = (I, Q, U, V), but we can't measure V since it requires a quarter wave plate, thus we obtain:

$$I^{det}_{j,k,m} = \sum_{n=1}^{N} (v_{j,k,1} * H_{j,k,m,n} * I_n + v_{j,k,2} * H_{j,k,m,n} * Q_n + v_{j,k,3} * H_{j,k,m,n} * U_n) \tag{2}$$

Let's denote base B as B = $(I^u_{star},\ I^u_{disk},\ Q,\ U)$
If we now focus on the point spread function $H_{j,k,l,m}$(PSF) :

$$H_{j,k,l,m} = \sum_{n'=1}^{N} (T_{j,k})_{m,n'} (A_k)_{n',n} \tag{3}$$

With A_k being a gaussian blur and $T_{j,k}$ the composition of a translation function λ and a rotation function ω, which can be expressed as:

$$T_{j,k}(x) = \lambda_{j,k}\omega_{j,k}x \tag{4}$$

If we apply $T_{j,k}$ to I_n, by denoting $I_n = I_{n,disk} + I_{n,star}$ we get :

$$T_{j,k}(I_n) = \lambda_{j,k}(\omega_{j,k}(I_n)) = \lambda_{j,k}(\omega_{j,k}(I_{n,disk} + I_{n,star}))$$

Because $\lambda_{j,k}$ and $\omega_{j,k}$ are linear, we have :

$$T_{j,k}(I_n) = \lambda_{j,k}(\omega_{j,k}(I_{n,disk})) + \lambda_{j,k}(\omega_{j,k}(I_{n,star}))$$

Since applying a rotation on the star has no effect as its diffraction pattern is a rotation invariant pattern, thus : $\omega_{j,k}(I_{n,star}) = I_{n,star}$

We deduce :

$$T_{j,k}(I_n) = \lambda_{j,k}(\omega_{j,k}(I_{n,disk})) + \lambda_{j,k}(I_{n,star})$$
$$T_{j,k}(I_n) = \lambda_{j,k}(\omega_{j,k}(I_{n,disk}) + I_{n,star})$$

Thus, obtaining :

$$T_{j,k}(I_n) = \lambda_{j,k}(\omega_{j,k}(I_{n,disk}) + I^u_{n,star}) \tag{5}$$

Finally if we come back on our model using (2), (3) and (5), we get :

$$\begin{aligned} I^{det}_{j,k}(B) = \sum_{m=1}^{N} v_{j,k,1} & \underbrace{\left\{ \sum_{n=1}^{N} \lambda_{j,k} \left[\omega_{j,k}(I_{disk} * A_k) + I^u_{star} \right]_{m,n} \right\}}_{=S_{1,j,k}} \\ & + v_{j,k,2} \underbrace{\left\{ \sum_{n=1}^{N} \lambda_{j,k} \left[\omega_{j,k}(Q * A_k) \right]_{m,n} \right\}}_{=S_{2,j,k}} \\ & + v_{j,k,2} \underbrace{\left\{ \sum_{n=1}^{N} \lambda_{j,k} \left[\omega_{j,k}(U * A_k) \right]_{m,n} \right\}}_{=S_{3,j,k}} \end{aligned} \tag{6}$$

5.2 Direct Model and Inverse Problem Approach

The direct model and inverse problem approach involves using a model to predict the data and then solving an inverse problem to estimate the disk's properties from the observed data. The objective is to minimize the cost function, which includes a data fidelity term and a regularization term (prior).

$$\min_{disk} \left(\underbrace{\text{distance}(\text{model}(disk), \text{ data}) + \lambda \, \text{prior}(disk)}_{\text{Cost Function}} \right) \tag{7}$$

6 Inverse problem

Starting from equation **(13)** from paper RHAPSODIE :

$$\hat{X} = \arg\min_{X \in C} \left\{ f(X) = (f_{data} + f_{prior})(X) \right\} \tag{8}$$

7 Data Fidelity Term

Based on equation **(14)** from paper RHAPSODIE, our data fidelity term is under the following form:

$$f_{data}(X) = \sum_{j,k} \| d_{j,k} - I^{det}_{j,k}(X) \|^2_{W_{j,k}} \tag{9}$$

where:

- d is the measured data
- I_{det} is the direct model
- W are the weights
- X represents the Stokes parameters $(I^u_{star}, I^u_{disk}, Q, U)$

Combining all of our results, we can now explicit our model in basis O:

$$I^{det}_{j,k}(S) = v_{j,k,1}(I^u_{star} + I^u_{disk} + I^p_{disk}) + v_{j,k,2}(Q) + v_{j,k,3}(U) \tag{10}$$

8 Gradient and Jacobian Matrices

8.1 Model's Gradient

We have :

$$\boldsymbol{\nabla} I^{det}_{j,k}(B) = \begin{pmatrix} v_{j,k,1}(1) \\ v_{j,k,1}(1) \\ v_{j,k,1}(\frac{Q}{\sqrt{Q^2+U^2}}) + v_{j,k,2}(1) \\ v_{j,k,1}(\frac{U}{\sqrt{Q^2+U^2}}) + v_{j,k,3}(1) \end{pmatrix} \tag{11}$$

8.2 Data Fidelity Term's Gradient

According to our previous results, we deduce the following gradient:

$$\nabla f_{data}(B) = \sum_{j,k} \nabla \left\| d_{j,k} - I_{j,k}^{det}(B) \right\|_{W_{j,k}}^2 \tag{12}$$

Jacobian of the Data Fidelity Function

We define $J_{S->B}$ as the jacobian that allows to go from $I_{j,k}^{det}(S)$ to $I_{j,k}^{det}(B)$
Thus having $\nabla I_{j,k}^{det}(B) = J_{S->B} * \nabla I_{j,k}^{det}(S)$
With our jacobian under the following form:

$$J_{S->B} = \begin{pmatrix} 1 & 0 & 0 & 0 \\ 0 & 1 & 0 & 0 \\ 0 & \frac{Q}{\sqrt{Q^2+U^2}} & 1 & 0 \\ 0 & \frac{U}{\sqrt{Q^2+U^2}} & 0 & 1 \end{pmatrix} \tag{13}$$

9 Regularization Terms (Prior Terms)

Two regularizations are used:

- **Edge-Preserving Smoothing**: Charbonnier et al. (1997)

$$\lambda f_{prior,disk}(I_{disk}^u, Q, U) = \lambda_{disk} \sqrt{\|\Delta Q\|^2 + \|\Delta U\|^2 + c\|\Delta I_{disk}^u\|^2 + \epsilon_{I_{disk}^u + I_{disk}^p}^2} - \epsilon_{I_{disk}^u + I_{disk}^p} \tag{14}$$

- **Tikhonov**: Tikhonov (1963)

$$\lambda f_{prior,star} = \frac{\lambda_{star}}{2\varepsilon_{star}} \|\Delta I u_{star}\|^2 \tag{15}$$

The main goal of the edge-preserving smoothing is, as its name indicates, preserving the edges of our image, here being the disk. On the other hand we won't apply it to the star part since we don't want to conserve it's edges. Thus applying Tikhonov, that is an uniform regularization. From now on we will call $f_{prior} = f_{prior,disk} + f_{prior,star}$

10 Results

10.1 Ground Truth

According to figure 2, the ground truth is simulated from DDiTOlofsson et al. (2020) disk data. This simulation helps validate the methods used in this study.

10.2 Under vs Over Regularization

As we can see in figure 3 and figure 4 the regularization parameter is impacting a lot our output. If it is set on a low value, our output will become blurry, on the contrary, if the value is too high, our output will become too noisy and have that grainy appearance.

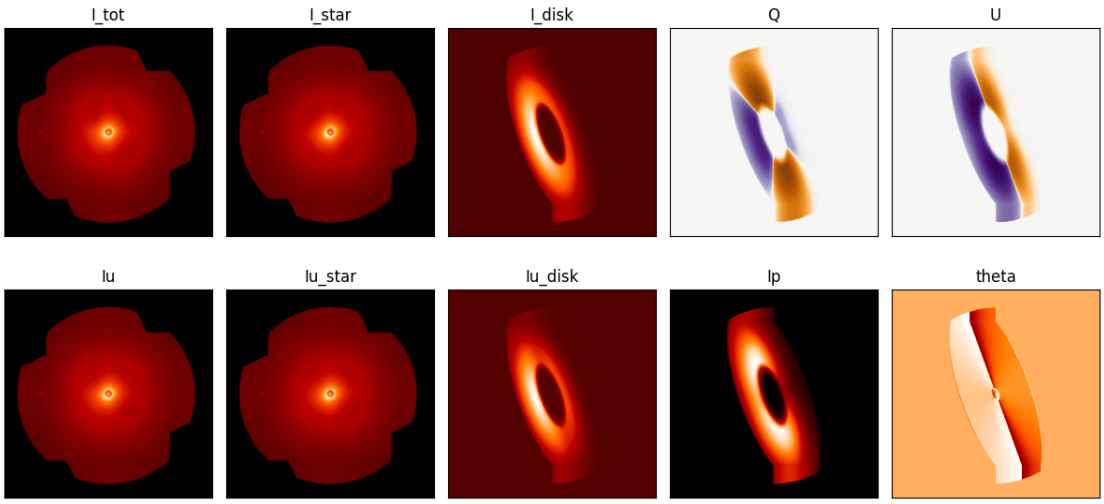

Figure 2: Ground truth simulated from DDiT disk

10.3 RMSE Comparison

According to figure 5, the Root Mean Square Error (RMSE) comparison for I^p between RHAPSODIE, ADIR, and Double Difference shows the performance of each method. According to figure 5, Rhapsodie is better than Double Difference (Double Difference is constant because it is not regularized). Furthermore ADIR seems a bit off, it is still under investigation but we suppose it comes from the ill-fitted contrast that still needs to be tuned.

10.4 Reconstruction Example

A reconstruction of the ground truth is shown (figure 6) to illustrate the effectiveness of the ADIR method. As we can see, ADIR is still struggling to detect and isolate the disk from the star (in I_disk), the main reason would probably come from the gradient that has been incorrectly implemented, since I used RHAPSODIE as my base code, the gradient might be wrong and needs to be change. For the other attributes, we can observe that ADIR is correctly reproducing the different image's components.

10.5 Methods Comparison on Simulated Data

The comparison between state-of-the-art methods on I^u, I^p, and θ is presented on figure 7, showing the relative performance of each method. The main thing to observe is that ADIR is the one presenting the least amount of the star in I^u thus being the closest to the ground truth, I^p seems to be a bit better on RHAPSODIE, considering that the double difference is way off the ground truth since it still contains the star. Finally for θ, ADIR seems to be as good as the double difference to reconstruct this part, whereas RHAPSODIE produce a result that is a bit blurry.

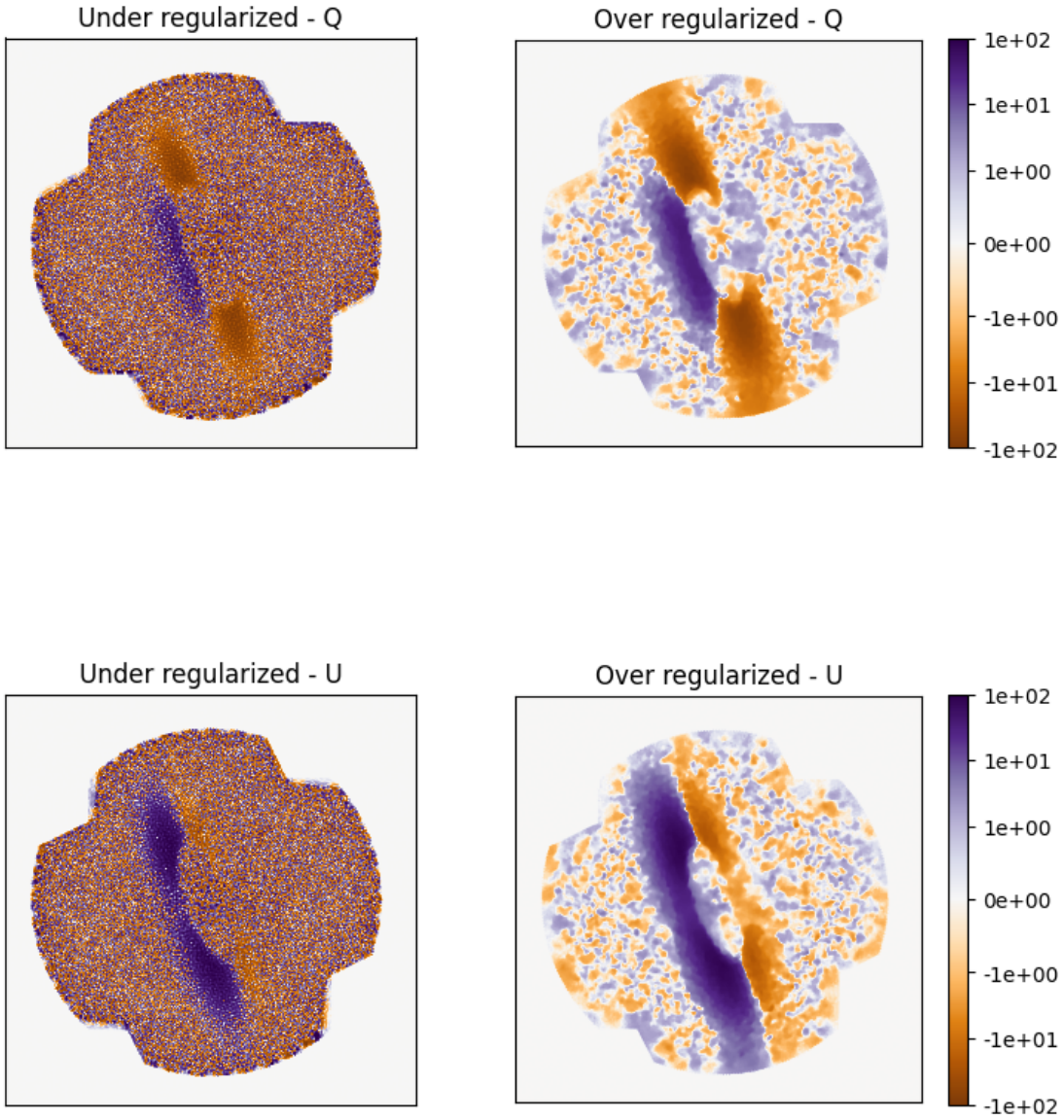

Figure 3: Comparison of under vs over regularization on Q and U

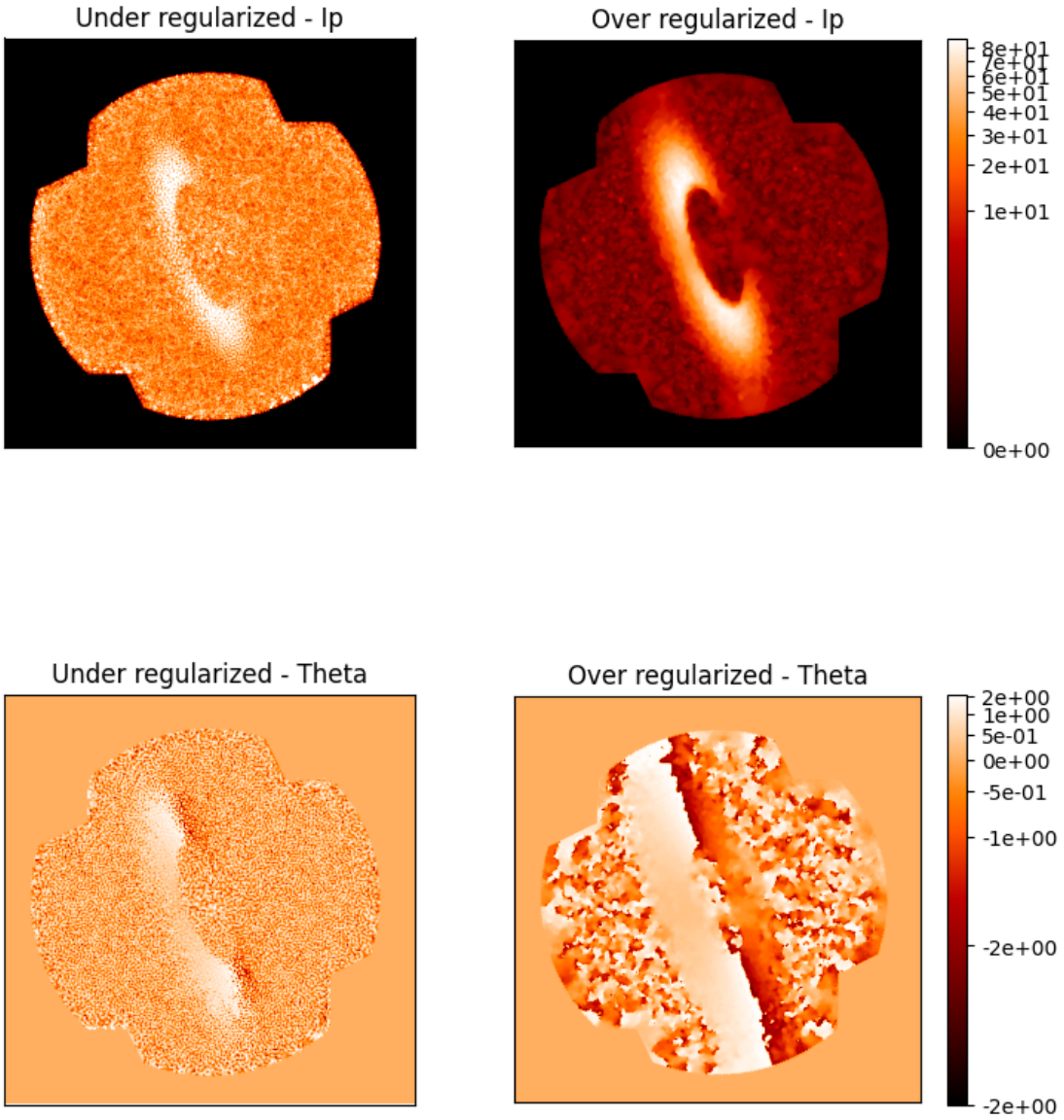

Figure 4: Comparison of under vs over regularization on θ

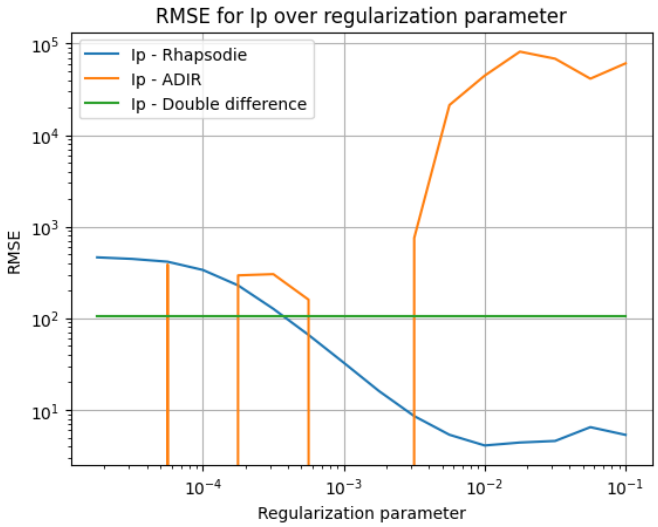

Figure 5: RMSE comparison for I^p between RHAPSODIE, ADIR, and Double Difference

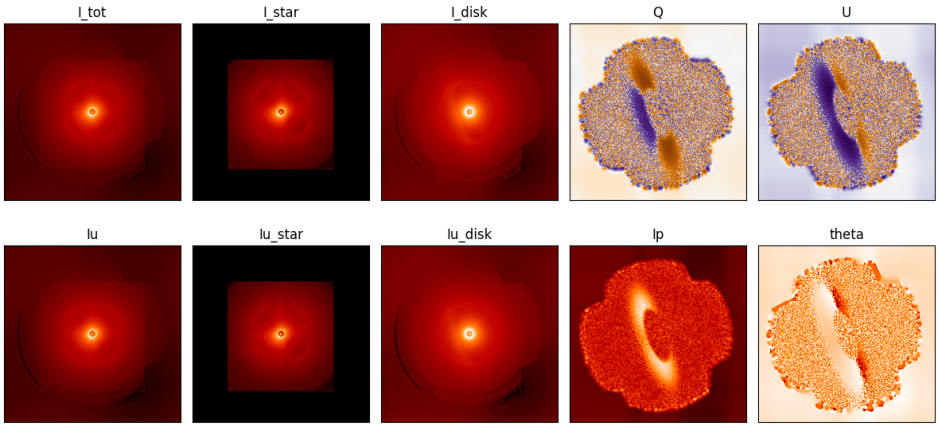

Figure 6: Reconstruction example of the ground truth

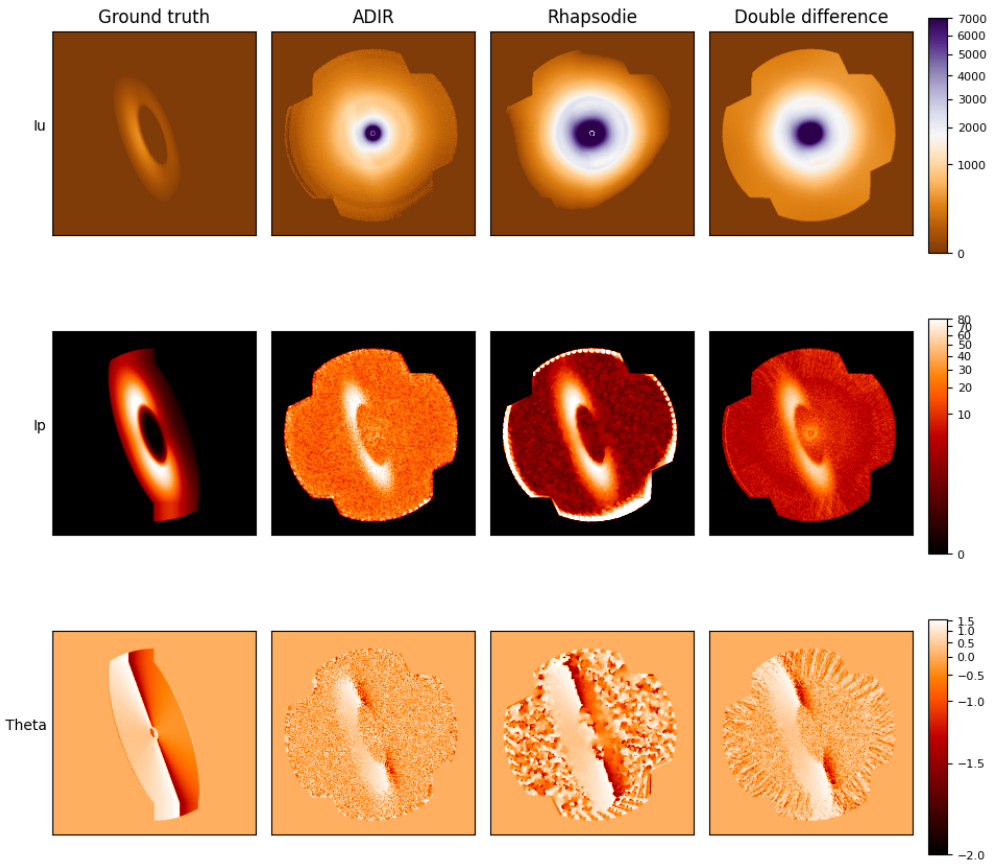

Figure 7: Comparison between state-of-the-art methods on I^u, I^p, and θ

11 Conclusion and Perspective

11.1 Conclusion

In this report, we addressed the challenge of observing circumstellar environments, which are crucial for understanding planet formation processes. These regions, surrounding young stars, require advanced observational methods to disentangle the bright starlight from the faint signals of surrounding disks. Two primary methods, Angular Differential Imaging (ADI) and Differential Polarization Imaging (DPI), have been highlighted for their effectiveness in this task.

My work focused on applying Angular Differential Imaging Reconstruction (ADIR) to simulated images to evaluate its performance in discriminating between the starlight and the light reflected by the circumstellar disk.

The first results obtained from the simulated images are promising. ADIR demonstrated a significant ability to partially discriminate the star's light reflected on the disk from the starlight. This discrimination is crucial for studying the properties and structures of circumstellar disks, which can provide insights into the early stages of planet formation.

The results indicate that ADIR can be effectively used in combination with high-contrast imaging instruments like ESO/VLT SPHERE IRDIS, which are designed to achieve detailed observations of faint circumstellar disks and exoplanets around bright stars. The application of ADIR in actual observations could significantly improve the quality of data obtained, enabling more precise studies of these complex environments.

In summary, my contribution lies in the potential of ADIR through simulations.

11.2 Perspective

Future work will focus on refining the ADIR technique and applying it to actual data from high-contrast imaging instruments. This will help in further enhancing our understanding of circumstellar environments and the processes leading to planet formation. The promising results from this initial study encourage continued development and testing of ADIR, with the goal of achieving more accurate and detailed astronomical observations in the future, also fine-tuning the hyperparameters, such as contrast and regularization parameters.
Furthermore, since both I^p and I^u are available, it is now possible to calculate the polarization ratio of different disks.

Chapter 1

Bibliography

Charbonnier, P., Blanc-Féraud, L., Aubert, G., and Barlaud, M. (1997). Deterministic edge-preserving regularization in computed imaging. *IEEE TIP*, 6(2):298–311. (page 9)

de Boer, J. and Langlois, M. (2020). Polarimetric imaging mode of VLT/SPHERE/IRDIS: I. Description, data reduction, and observing strategy. *Astronomy & Astrophysics*, 633:A63. (page 3)

de Boer, J., Langlois, M., van Holstein, R. G., Girard, J. H., Mouillet, D., Vigan, A., Dohlen, K., Snik, F., Keller, C. U., Ginski, C., Stam, D. M., Milli, J., Wahhaj, Z., Kasper, M., Schmid, H. M., Rabou, P., Gluck, L., Hugot, E., Perret, D., Martinez, P., Weber, L., Pragt, J., Sauvage, J.-F., Boccaletti, A., Le Coroller, H., Dominik, C., Henning, T., Lagadec, E., Ménard, F., Turatto, M., Udry, S., Chauvin, G., Feldt, M., and Beuzit, J.-L. (2020). Polarimetric imaging mode of VLT/SPHERE/IRDIS: I. Description, data reduction, and observing strategy. *A&A*, 633:A63. (page 3)

Denneulin, L. (2021). RHAPSODIE: Reconstruction of High-contrAst Polarized SOurces and Deconvolution for cIrcumstellar Environments. *Astronomy & Astrophysics*. (page 3)

Marois, C. (2006). Angular Differential Imaging: a Powerful High-Contrast Imaging Technique. *The Astrophysical Journal*. (page 3)

Olofsson, J., Milli, J., Bayo, A., Henning, T., and Engler, N. (2020). The challenge of measuring the phase function of debris discs. Application to HR 4796 A. *Astronomy & Astrophysics*, 640:A12. (page 9)

Tikhonov, A. N. (1963). Regularization of incorrectly posed problems. Soviet Mathematics Doklady. (page 9)

Tinbergen, J. (2005). Astronomical polarimetry. *Astronomical Polarimetry*. (page 3)